ELSEVIER

Journal of Magnetism and Magnetic Materials 171 (1997) 16–28

Journal of magnetism and magnetic materials

Strain-induced perpendicular magnetic anisotropy in ultrathin Ni films on $Cu_3Au(0\,0\,1)$

A. Braun*, B. Feldmann, M. Wuttig

Institut für Grenzflächenforschung und Vakuumphysik, Forschungszentrum Jülich GmbH, D-52425 Jülich, Germany

Received 26 August 1996; received in revised form 20 December 1996

Abstract

We have investigated magnetism, morphology and structure of nickel films grown on $Cu_3Au(0\,0\,1)$ to explore the potential of modifying magnetic anisotropies by epitaxial strains. Ultrathin films from the submonolayer region up to 55 monolayers (ML) were grown epitaxially on a $Cu_3Au(0\,0\,1)$ single crystal. Layer-by-layer growth is observed up to 10 ML. A quantitative analysis of the low-energy electron diffraction (LEED) pattern reveals coherent film growth up to 5 ML. Between 5 and 8 ML the in-plane lattice constant is reduced by 4%, which corresponds to a reduction of the film strain by 70%. This is accompanied by an increase in the interlayer spacing, which is in quantitative agreement with predictions of linear elasticity theory. Kerr measurements show that the films have an in-plane magnetization in the thickness region from 3 to 5 ML and for thicknesses larger than 12 ML. Between 5 and 12 ML a perpendicular anisotropy is observed which is particularly pronounced between 8 and 10 ML. This reorientation of the magnetization direction is caused by the coherency strain in the film.

PACS: 61.50.Ks; 68.35.Rh; 75.30.Gw; 75.50.-y; 75.70.Ak

Keywords: Perpendicular magnetic anisotropy; Magnetoelasticity; Epitaxial strain; Ni thin films; Structure and magnetism

1. Introduction

It is well known that thin film properties often deviate considerably from the properties of the corresponding bulk material. This offers interesting opportunities for technical applications. In magnetic storage media, the quest for materials with a perpendicular magnetic anisotropy is an ongoing research effort. A variety of approaches has been explored to stabilize a perpendicular magnetic anisotropy [1]. Elastic strain due to epitaxial growth of thin films leads to changes in the total energy of a ferromagnet, and thus, can change the magnetic anisotropy by magnetoelastic effects. Experimental

* Corresponding author. Present address: Paul Scherrer Institute, Electrochemistry Section, CH-5232 Villigen PSI, Switzerland. Tel.: + 41 56 310 2128; fax: + 41 56 310 4415; e-mail: artur.braun@psi.ch.

0304-8853/97/$17.00 © 1997 Elsevier Science B.V. All rights reserved
PII S0304-8853(97)00010-3

evidence for this behaviour has been found for epitaxial Ni films on Cu(0 0 1), which show a perpendicular magnetic anisotropy between 12 and 75 ML [2–4]. The reorientation of the easy magnetic axis has been attributed to the coherency strain in the nickel films. Nickel has a lattice constant of 3.524 Å, while that of copper is 3.61 Å. The resulting lattice mismatch is less than 2.5%. As Cu_3Au(0 0 1) has a lattice constant of 3.745 Å, the lattice mismatch of nickel on this substrate is 6.3%.

According to elasticity theory, in the case of pseudomorphic growth, the Ni should grow in a face-centered tetragonal phase on Cu_3Au(0 0 1); see Refs. [5, 6]. Due to the large mismatch for this growth mode, the switching thickness from in-plane to perpendicular easy axis should be much smaller than in the case of Ni/Cu(0 0 1).

2. Experimental

All experiments were performed in an ultrahigh vacuum (UHV) chamber which has already been described elsewhere [7]. The chamber is equipped with a low-energy electron diffraction (LEED) and medium-energy electron diffraction (MEED) system, a cylindrical mirror analyzer (CMA) for Auger analysis and a pair of Helmholtz coils to apply a magnetic field up to 1 kOe. The base pressure in the UHV chamber is 3×10^{-9} Pa. A polished Cu_3Au(0 0 1) single crystal was used as a substrate, with a surface orientation better than 0.1° against the (0 0 1) surface normal. After cleaning by Ar-ion etching at 2 keV and annealing cycles up to 775 K, the contamination level was below the detection limit of the Auger system. The Cu_3Au substrate showed the sharp and well-known c (2×2) LEED-pattern, due to the chemical order of the Cu and Au sublattices which exists below the order/disorder transition at 663 K [8]. The evaporation source was a thin Ni-platelet of 10 mm diameter, 0.2 mm thickness and 99.98% purity, heated by radiation of a tungsten filament. During evaporation, pressure did not exceed 2×10^{-8} Pa. The growth of the films was monitored by MEED, employing electron energies of 3 keV at an angle of incidence of around 5° against the surface. The resulting diffraction pattern was displayed on the fluorescent screen of the LEED system. The intensities of up to 8 diffraction spots were measured simultaneously using a videocamera and a PC data acquisition system. As the MEED curves showed layer-by-layer growth, it was possible to provide a calibration curve for thickness determination. The oscillation period corresponds to the time necessary for one monolayer to complete [9, 10]. From this quantity the evaporation rate was determined. Using this evaporation rate, which was checked to be constant to within ±3%, Auger spectra were recorded as a function of nickel coverage. Fig. 1 shows the intensity ratio of the Auger peak at 848 eV, predominantly a Ni Auger transition, and the Cu Auger peak at 920 eV as a function of film thickness. The solid line represents the best fit to the data. In the following we have used the Auger intensity ratio of an arbitrary film to determine its thickness. This is particularly helpful when characterizing wedge-shaped films which allow for a fast correlation of growth, structure and magnetism. Since the Kerr rotation is rather small for nickel, the measurement of hysteresis loops becomes difficult for ultrathin films of a few ML with a more conventional setup. To improve sensitivities, we have recorded the dynamic magnetic susceptibility as described in Refs. [11, 12]. The susceptibility has its

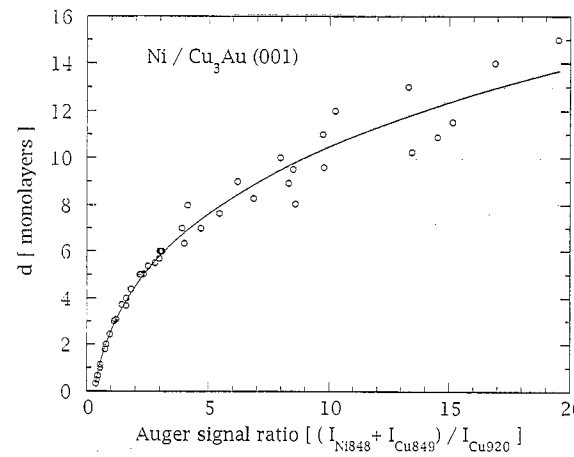

Fig. 1. Thickness calibration curve for Ni films on Cu_3Au(0 0 1). The circles show the ratio of Auger signals from film and substrate, depending on film thickness. The solid line represents the best fit to the data.

maximum value at the Curie temperature. This method was applied to films from 2 to 15 ML.

3. Results and discussion

3.1. Film growth

A number of MEED curves was recorded for different growth conditions. Films were grown at deposition rates between 0.3 and 2.4 ML/min and sample temperatures of 100, 200 and 300 K. Fig. 2 shows the MEED curve of the specular beam at 300 K. The characteristic features of this curve are deep intensity minima at 1 and 5 ML, regular intensity oscillations between 2 and 5 ML and between 7 and 11 ML and another broad intensity minimum between 12 and 16 ML. Regular intensity oscillations are the characteristic feature of layer-by-layer growth [9, 10]. This raises the question what causes the intensity minima at 1 and 6 ML and above 12 ML. To answer this, the film morphology was also analyzed with LEED. Around 1 ML thickness, an energy-dependent broadening of the LEED spots is observed which indicates that the films have a high step density. This is in line with the high surface free energy of Ni (2.08 J m^{-2}), which exceeds the surface free energy of the substrate components Cu (1.57 J m^{-2}) and Au (1.33 J m^{-2}). Hence, Ni does not want to wet the Cu_3Au substrate. This explains the intensity minimum around 1 ML. A very similar film growth has been observed for the first five ML of Fe on Cu(0 0 1), where again the energetics favour a non-wetting film growth [13].

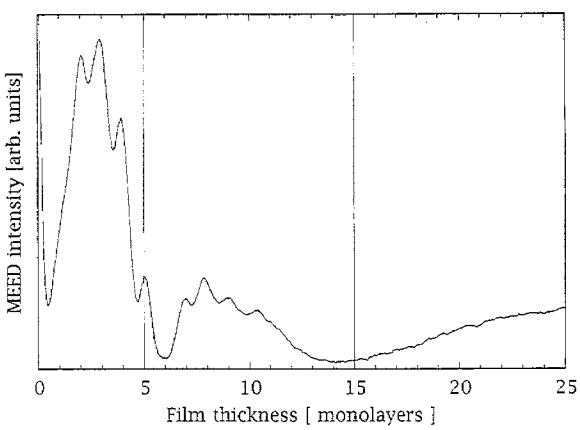

Fig. 2. MEED intensity of the specular beam at 300 K sample temperature. Regular intensity oscillations between 2 and 5 ML and between 7 and 11 ML indicate layer-by-layer growth. While the intensity minimum at 1 ML is caused by a high step density, the minimum at 6 ML is caused by changes in film structure.

The intensity minimum at 6 ML must have a different origin, however. This is shown by LEED observations of an oscillating width of the specular beam as a function of energy in this thickness range. On a wedge-shaped sample an oscillation of the broadening of the specular beam could be observed, depending on film thickness. While sharp spots were observed at thicknesses of 5, 6 and 7 ML, broad and diffuse spots are seen at 4.5, 5.5 and 6.5 ML for selected energies. This is the characteristic feature we expect for layer-by-layer growth [14, 15]. Presumably, the minimum in the MEED curve at 6 ML is therefore caused by other effects such as changes in film structure. This is also supported by growth experiments at lower sample temperatures. MEED curves recorded at 200 and 100 K show no intensity oscillations, indicating that at these growth temperatures the nickel adatom mobility is not sufficient to sustain layer-by-layer growth. Nevertheless, both MEED curves show a clear intensity minimum between 5 and 6 ML, which gives evidence for a similar structural change in this thickness range for all growth temperatures.

Finally, we want to point out that the oscillation amplitude in the MEED curves is decreasing with film thickness. This might be related with an Au segregation to the film surface. The Auger data show a small but discernible Au signal even for films up to 8 ML. The intensity of the gold Auger transition at 69 eV is decreasing with film thickness and vanishes around 12 ML. Possibly these Au atoms act as surfactants, allowing layer-by-layer growth of the nickel films. Such a scenario would explain the decreasing MEED oscillation amplitude with a decreasing number of Au atoms on the film surface with growing film thickness.

3.2. Structure

The structure of the films was investigated by LEED. Only films grown at room temperature

were investigated. After evaporation, the samples were cooled down to 90 K to obtain a sharp and intense diffraction pattern. For films up to 1.5 ML, the c (2×2) LEED pattern of the substrate is still visible. Above this coverage only a (1×1) LEED pattern is observed. An analysis of wedge-shaped films shows that between 1.5 and 5.5 ML the LEED spots of the (1×1) structure do not change their position with varying thickness. This implies that in this film thickness regime the nickel films grow pseudomorphic on the substrate surface. Above 5.5 ML, satellite spots occur at larger k-values in the vicinity of the substrate spots. They 'move' in FCC [0 1 1]-direction with increasing thickness. To determine the interatomic spacing in the film, LEED profiles were taken for a variety of thicknesses. For a square lattice, there is a particularly simple relation between unit vectors in real space, (a_i, a_j) and reciprocal space, (k_i, k_j): $k_i \cdot a_j = 2\pi\delta_{ij}$, and thus, $a_2 = a_1 \cdot k_1/k_2$. Here, k_1 is proportional to the distance between the (1 0) spot and the specular beam; k_2 is proportional to the distance between the satellite spot and the specular beam; a_1 corresponds to the lattice constant of the Cu_3Au-substrate, 3.745 Å. k_1 and k_2 are determined from diffraction profiles, such as the one shown in Fig. 3 which displays a LEED intensity profile of a 6.3 ML film. The profile is taken along the FCC

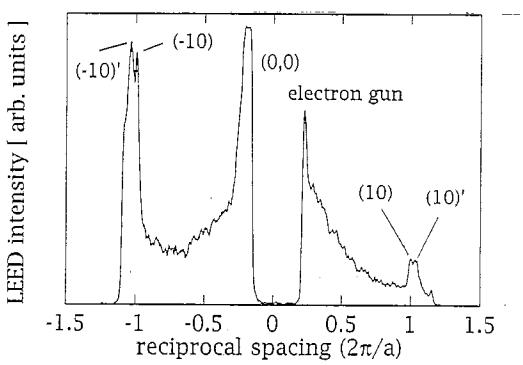

Fig. 3. LEED intensity profile of a 6.4 ML film, taken along the FCC (1 1 0)-direction. The genuine (1 0) spot and ($\bar{1}$ 0) spot correspond to the pseudomorphic Ni phase with an in-plane lattice spacing of 3.745 Å. The (1 0) spot and ($\bar{1}$ 0) spot correspond to a relaxed film phase with a smaller in-plane lattice spacing. The intensity between the ($\bar{1}$ 0) spot and the (1 0) spot is caused by the (0 0) beam and the electron gun.

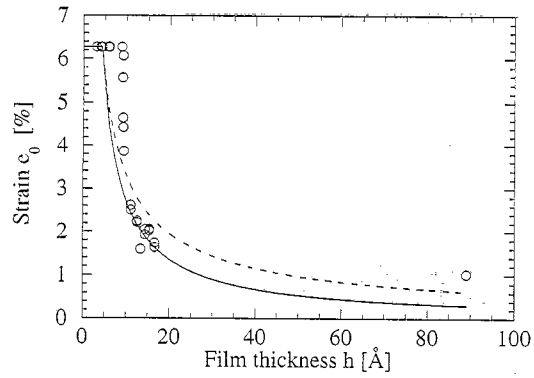

Fig. 4. Dependence of film strain $e_0 = (a_0 - a_{\parallel})/a_0$ in % upon film thickness in Å. The open circles are derived from the position of intensity maxima such as the ones shown in Fig. 3. These maxima do not shift below approximately 9 Å, decreasing in-plane spacings are observed above this thickness. The data point at 90 Å comes from a full dynamical LEED analysis [15]. The solid and broken lines describe theoretical predictions for the film strain. The solid line corresponds to $e_0(h) = \eta h_c/h$ for $h > h_c$ and $e_0(h) = h$ for $h < h_c$, as suggested by Ref. [17]. The broken line describes a fit ansatz as used by Ref. [16], i.e. $e_0(h) = m/h^a$, where a and m are fit parameters. In our case the best fit is obtained for $m = 18.8$ and $a = 0.76$.

[0 1 1]-direction. From this analysis, the nearest-neighbour spacing in the film can be determined with considerable precision (Fig. 4). These measurements confirm coherent growth up to 5.5 ML. Between 5.5 and 8 ML, the in-plane spacing is reduced to approximately 3.6 Å. This value is still larger than the lattice constant of FCC nickel (3.52 Å), hence, at this thickness the film is not fully relaxed to its bulk structure yet.

According to elasticity theory, changes in the in-plane spacing should be accompanied by changes in the interlayer spacing. To detect such changes, a series of LEED $I(V)$ curves for films of different thickness (Fig. 5) was recorded. Both the peak positions and the width of the peaks change with increasing film thickness. Particularly broad peaks are observed between 6 and 10 ML. The corresponding LEED pattern displays broad spots indicative for a high degree of disorder. Above 11.5 ML, the maxima in the $I(V)$ curves become narrower and the corresponding LEED pattern displays sharper spots. This shows that the structural order of the film is improving considerably

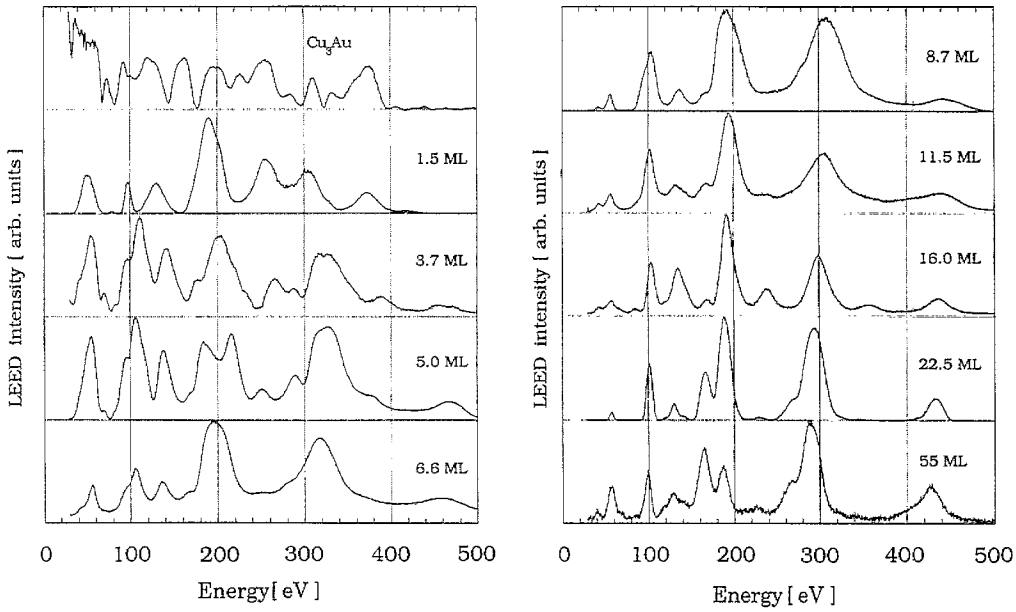

Fig. 5. LEED-$I(V)$ curves of the specular beam for different film thicknesses. Changing peak positions and peak widths indicate changes of film structure.

above 11 ML. These data have been compared with full dynamical calculations which will be presented elsewhere [16]. Here we will discuss a much simpler analysis of the data. The intensity of the specular beam, which is most sensitive to changes of the interlayer distance d_z, was recorded close to normal incidence. Within the kinematic theory, the interlayer spacing of the film can be determined from the energies where the intensity has a maximum in the LEED $I(V)$ curves. If the electron beam encloses the angle Θ with the surface normal, the maximum of the diffracted intensity of order n is found at an electron energy E_n, given by the following equation, if dynamic scattering processes are neglected:

$$E_n = n^2 \frac{150.4}{4d_z^2 \sin^2 \Theta} + \phi_0, \tag{1}$$

where ϕ_0 is the inner potential of the film. With increasing thickness, the peaks move towards positions of lower energy, which corresponds to an increasing interlayer distance of the films according to Eq. (1). The resulting interlayer spacings are displayed in Fig. 6. The data have to be considered

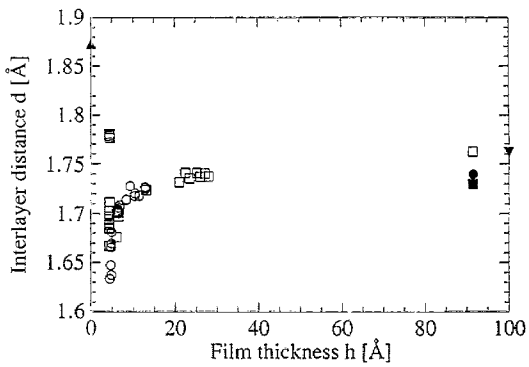

Fig. 6. Interlayer spacing of the Ni films in Å as a function of film thickness in Å. The open squares describe data points derived from the kinematic analysis of I/V curves. The solid square is the data point for a thick film determined by a full dynamical LEED analysis. For reference purposes the bulk interlayer spacing of $Cu_3Au(0\,0\,1)$ and Ni(0 0 1) is displayed as a solid triangle pointing up and down, respectively. The open circles describe interlayer spacings determined from the in-plane spacing in conjunction with the epitaxial line. The solid circle comes from a_0 as derived by a full dynamical LEED analysis. It is evident that above 10 Å the data points for the interlayer spacing as determined by the two different approaches agree fairly well.

with considerable caution. For very thin films the influence of the substrate has to be taken into account. Therefore, only films thicker than approximately 5 ML are considered in the following. The increase of the interlayer spacing of the film is accompanied by a decrease of the in-plane spacing. This is characteristic for the structural transformation towards relaxed and strain-free bulk nickel films. Yet, the kinematic analysis implies that even at 20 ML thickness the films are not yet fully relaxed. This is supported by the full dynamical LEED $I(V)$ analysis for a 55 ML thick film which determines the bulk interlayer spacing to 1.73 Å and the in-plane lattice constant to 3.56 Å [16]. These values are slightly smaller, respectively larger, than the corresponding strain-free interlayer spacing of 1.76 Å and the in-plane lattice constant of 3.52 Å, respectively. This corroborates the conclusion of the kinematic analysis of interlayer spacing and the determination of in-plane spacings from LEED profile measurements that even films at 20 ML and above are not yet completely relaxed. For a more quantitative understanding of the biaxial film strain and the interlayer spacing as a function of film thickness h, we compare our experimental data with theoretical predictions. The corresponding theory is described in detail in Ref. [17] and references therein. For Ni on $Cu_3Au(0\,0\,1)$, with a misfit η of 6.3%, a critical thickness for dislocation formation h_c of 4.3 Å (=2.3 ML) is expected. Below this thickness, Ni films should grow with a constant in-plane strain of $e_0 = \eta$. Above this thickness, the strain can be approximated by [18]

$$e_0(h) = \eta \frac{h_c}{h}, \quad h > h_c. \tag{2}$$

These predictions from theory are displayed as a solid line in Fig. 4, together with the experimental data. One can see that the experimental data points above 10 Å are described fairly well by the theoretical predictions. The error bar for each of these data points is $\pm 0.6\%$ for a_0. The data point at approximately 90 Å comes from the full dynamical LEED analysis of in-plane and interlayer spacings of a thick Ni film on $Cu_3Au(0\,0\,1)$ [16]. Here the error bar is approximately $\pm 0.9\%$. All data points above 10 Å agree fairly well with the predictions of theory. Discrepancies between theory and experiment are observed for films with thicknesses below 10 Å. Theory ([17] and references therein) would predict the formation of misfit dislocations above a critical film thickness of 4.3 Å. Experimentally only above 9 Å a substantial change of in-plane spacings is observed, however. Two possible explanations can be given to account for the discrepancies between theory and experiment. First of all, the analysis of in-plane spacings is based on the analysis of diffraction scans such as the one shown in Fig. 3. From the position of the maximum of intensity of the diffraction peak the in-plane spacing is derived. Above approximately 2.3 ML, in these profile measurements an increase of intensity adjacent to the (1 0) diffraction peaks at larger wave vectors is observed. This is indicative for the formation of a phase with smaller in-plane spacing as expected for the onset of dislocation formation. However, since the intensity maximum does not yet shift its position, Fig. 4 displays an unchanged in-plane spacing up to 9 Å. Furthermore the question arises how well linear elasticity theory can describe the behaviour of ultrathin films with a considerable misfit of approximately 6%. Bochi et al. [17] have recently determined the strain of Ni films on Cu(0 0 1) and on a $Cu_{1-x}Ni_x(0\,0\,1)$ surface. They fit their film strain data by a slightly modified version of Eq. (2), i.e. $e(h) = m/h^a$, where a and m are fit parameters. We have also tried to fit our data with such an ansatz. The best fit we obtained is displayed as a broken line in Fig. 4 as well. Even though this fit gives a slightly better agreement at smaller thicknesses, it does not lead to a substantial overall improvement. Using linear elasticity theory, one cannot only determine the critical thickness for dislocation formation and the film strain as a function of film thickness, but one can also derive the interlayer spacing of the film from the misfit strain and the elastic constants. The corresponding relationship between film strain and interlayer spacing is called the epitaxial line [6]. We have used this relationship to determine the interlayer spacing of the Ni films from the in-plane spacings displayed in Fig. 4. The resulting interlayer spacings are displayed in Fig. 6 together with the results of interlayer spacings obtained directly from an analysis of LEED

I/V curves. The open squares describe the interlayer spacing as obtained from a kinematic analysis of peak positions (Eq. (1)). The solid square describes the bulk interlayer spacing of a thick Ni film as obtained by a full dynamical LEED analysis [16]. Open circles display the interlayer spacing as derived from the in-plane spacing using the epitaxial line. All error bars are of the order of $\pm 1\%$. One can see that above film thicknesses of 10 Å the interlayer spacing of Ni film determined directly and via the epitaxial line agree nicely. Substantial discrepancies are found below 10 Å, but here the kinematic analysis to determine interlayer spacings does not give reliable data. Hence, we can conclude that both ways to derive interlayer spacings of Ni films above thicknesses of 10 Å lead to very consistent data.

3.3. Magnetism

To investigate the magnetic properties of the films, hysteresis loops for different film thicknesses were recorded from wedge-shaped samples (Fig. 7). The films were grown at room temperature, the hysteresis loops were measured by MOKE at a sample temperature of 166 K. For films below 5 ML, the signal was within the detection limit of our MOKE system. To increase sensitivity, the experimental set-up was modified as described in Refs. [11, 12] to detect the film magnetization even at 3 ML. With this technique the dynamic magnetic susceptibility is measured. From such data of the susceptibility as a function of sample temperature the Curie temperature can be determined. Fig. 8 shows the Curie temperature of the films depending on film thickness, for both polar and longitudinal geometry. For films with thicknesses between 8 and 12 ML, no signal was detected in longitudinal geometry, but in polar geometry. As illustrated in Fig. 9, in a medium thickness range between 7.5 and 12 ML, no signal for saturation magnetization was detected in longitudinal geometry, giving evidence for a perpendicular magnetized sample in this thickness range. Signals in polar geometry were detected from 5 to 12 ML, and the hysteresis loops had rectangular shape from 7.5 to 12 ML. This confirms the perpendicular anisotropy in this thickness range. In the vicinity of 5 ML, signals were also detected in longitudinal geometry, indicating the reorientation transition in this region. In particular, the measurements of magnetic susceptibilities show that between 3 and 5 ML the films are magnetized in-plane. The same holds for film thicknesses above 12 ML where no polar, but a longitudinal signal is detected. The hysteresis loops in this geometry have a rectangular shape above 20 ML. The slope of the Kerr ellipticity as a function of film thickness in the regime 5–12 ML and above 12 ML remains constant, which is a sign for a homogeneously magnetized film. As the sensitivity of the Kerr effect is much larger for polar measurements, a dominant in-plane magnetization should exist at those thicknesses, where a longitudinal signal is detected mainly. Thus, the switching thicknesses are at approximately 6.5 and 12 ML. Such a twofold reorientation has also been observed for Ni films on Cu(0 0 1) [2–4]. But it is clear that the reorientation is a continuous transition in the sense that it takes place over a finite thickness range. In the next section, we will show that a similar driving force governs the reorientation of the magnetic anisotropy for both epitaxial systems. In the appendix, we describe how the various contributions of the magnetic anisotropy affect the direction of the magnetization vector.

3.4. Correlation of magnetism, morphology and structure of the Ni films

Fig. 10 summarizes experimental findings for the growth, structure and magnetism of the films. The MEED curve in the top portion of Fig. 10 is characterized by regular intensity oscillations indicative for layer-by-layer growth up to 11 ML. Pronounced minima are observed at 1 and 5 ML. While the former minimum is related to a rough surface, the latter is not connected with a rough film morphology, but must have a different origin. The analysis of the film structure indicates that a change in film structure rather than a morphological change could explain this minimum. The in-plane lattice spacing, displayed in the centre of Fig. 10, shows a pronounced decrease for thicknesses around 5.5 ML. This gives evidence that the film stress is relieved at this thickness by the formation of misfit dislocations. The resulting structural

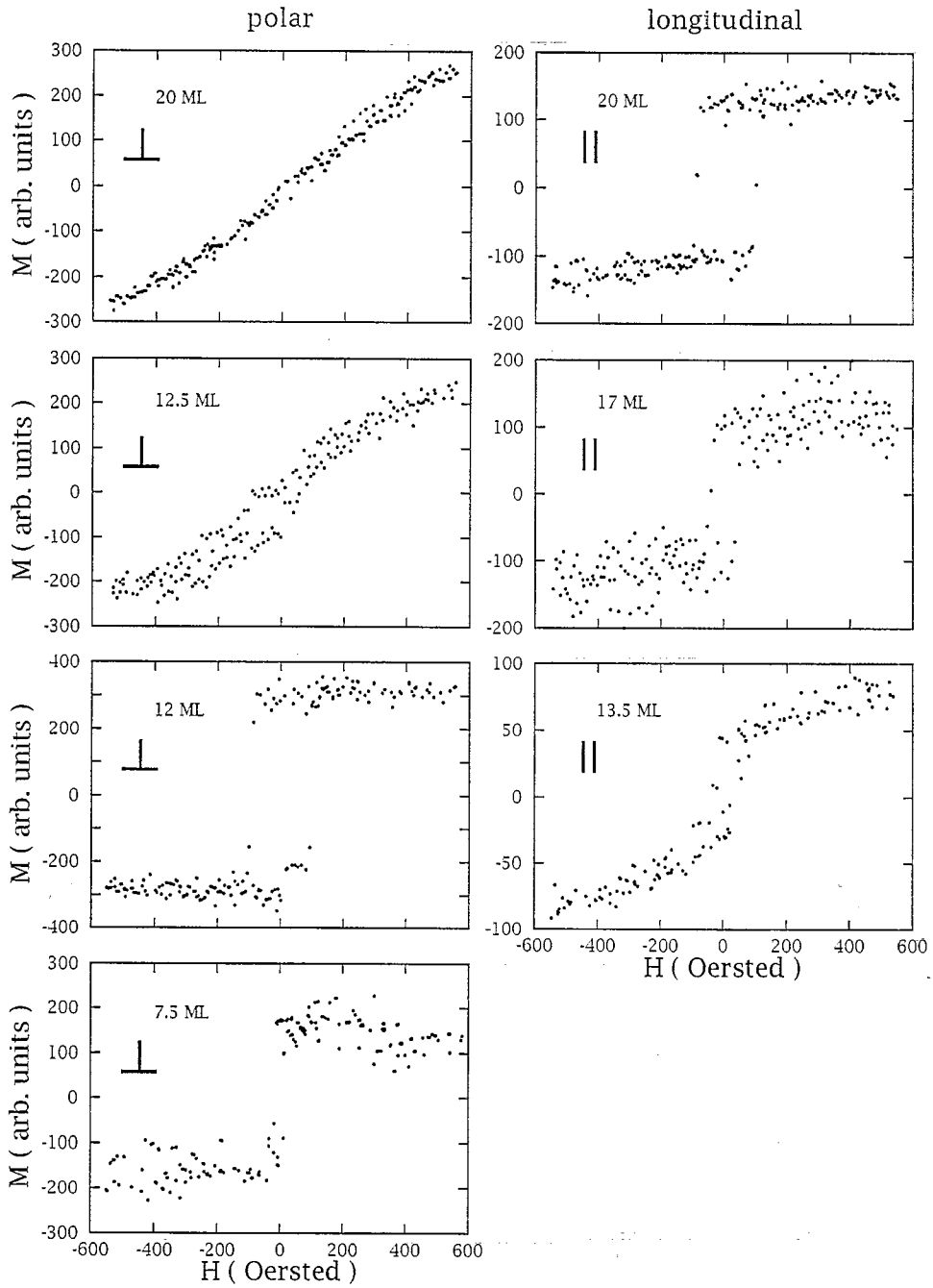

Fig. 7. Kerr hysteresis loops for chosen film thicknesses in polar and longitudinal geometry. In polar geometry, the loops have rectangular shape up to 12 ML. With increasing thickness, the loops become rectangular in longitudinal geometry at approximately 20 ML.

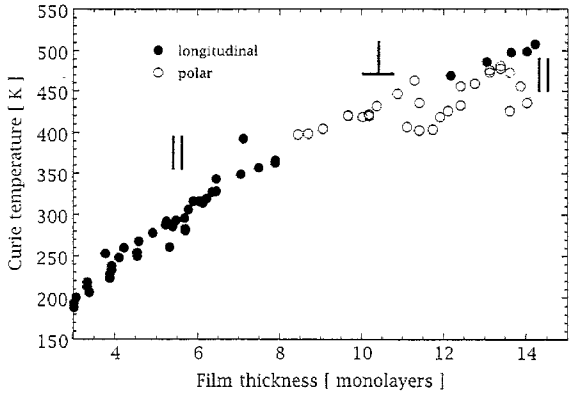

Fig. 8. Curie temperature as a function of film thickness. Between 8 and 12 ML, no signals were measured in longitudinal geometry, but in polar geometry.

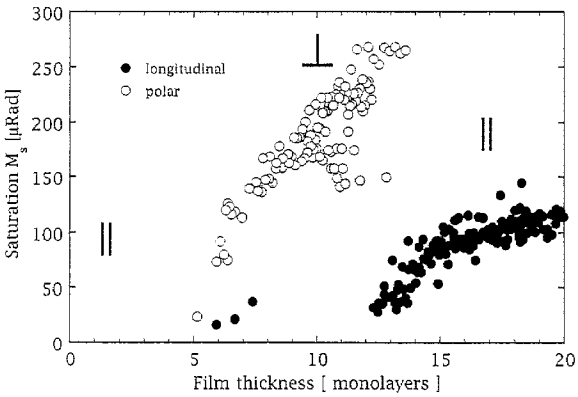

Fig. 9. Saturation magnetization of the samples, measured for both Kerr geometries. Absence of signals in longitudinal geometry and presence of signals in polar geometry between 8 and 12 ML indicate a pronounced out-of-plane magnetization.

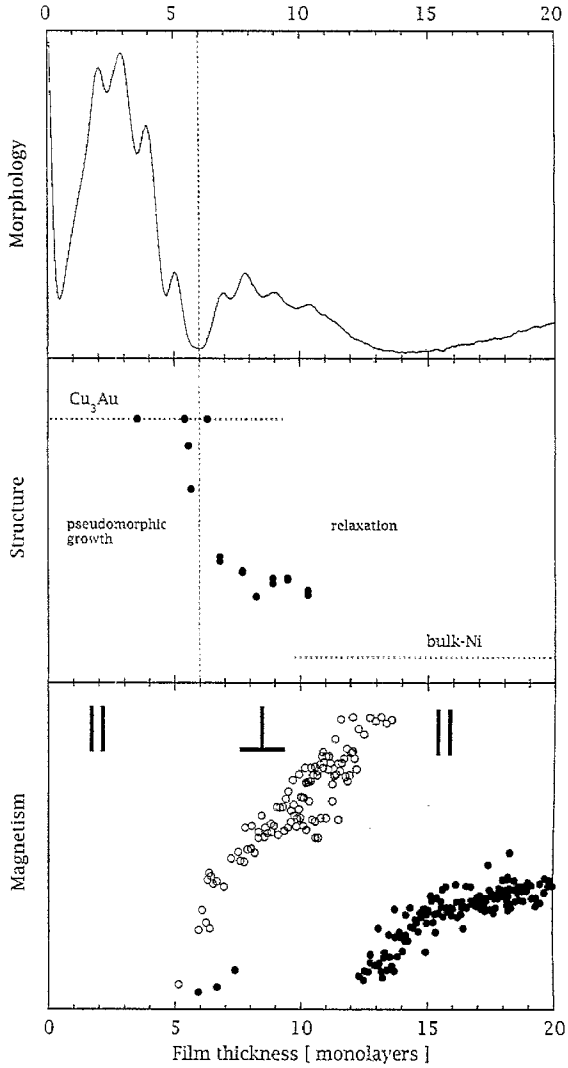

Fig. 10. Comparison and correlation of morphology, structure and magnetism for Ni films on $Cu_3Au(0\,0\,1)$.

disorder of the films could both explain the broad maxima of the LEED $I(V)$ curves between 5 and 8.5 ML and the MEED intensity minimum around 5 ML. Connected with these findings is the change of in-plane lattice spacing around 5 ML, which is expected once the film starts to relax the epitaxial stress by dislocation formation. From linear elasticity theory the critical thickness can be calculated for which dislocation formation becomes energetically favourable [19]. For the growth of pseudomorphic Ni films on Cu(0 0 1) the misfit is 2.45%, leading to a calculated critical thickness of 18 Å [17]. For the growth of pseudomorphic Ni films on $Cu_3Au(0\,0\,1)$ the misfit is 6.3%, leading to a calculated critical thickness of 4.3 Å (=2.3 ML). This value is considerably smaller than the thickness where we observe a change in in-plane spacing. Yet, beam profiles measured for thicknesses above 2 and below 5 ML already, show a weak LEED intensity at k-values larger than those arising from the substrate. This indicates that above 2 ML already, parts of the film start to relax until a more massive rearrangement

proceeds around 5 ML. Hence, the films between 2 and 5 ML are no longer fully strained.

The resulting stress contributes through the magnetoelastic energy to the magnetic anisotropy. Calculations which are described in detail in the appendix determine the reorientation thickness of the magnetization to approximately 3.5 ML. This estimate, however, is based on a pseudomorphic and, hence, fully strained nickel film. Experimentally, the reorientation is only observed around 5.5 ML, in qualitative agreement with the reduced film stress. For a quantitative comparison between experiment and theory one would need to know the film strain precisely. Unfortunately, our present analysis of the film structure does not allow to determine this strain with sufficient precision in this particular thickness regime. Hopefully, our full dynamical LEED analysis will allow a more detailed characterization of both in-plane and interlayer spacings. An alternative approach would be high-resolution electron or X-ray diffraction, possibly in conjunction with techniques that directly measure the film stress [20].

It is interesting to compare the present finding with the behaviour of nickel films on Cu(0 0 1). For this system the magnetic reorientation is observed for thicknesses between 10 and 12 ML [2–4]. The larger reorientation thickness is in qualitative agreement with the smaller film strain, caused by the lattice mismatch of 2.5% between nickel and copper. From theory we know that epitaxial Ni films have a larger magnetic reorientation thickness, the smaller the lattice mismatch is. This is confirmed, if we consider the system Ni on Cu(0 0 1) [2–4], where the first reorientation is between 10 and 12 ML. Our calculation as described in the appendix determines the reorientation thickness to approximately 11 ML. This excellent agreement might be somewhat fortuitous however, since any formation of dislocations should decrease the strains of the Ni films [19] and, hence, change the reorientation thickness.

4. Summary

Epitaxial Ni films up to 55 ML have been grown on $Cu_3Au(0\,0\,1)$ at room temperature. Up to 5 ML, these films are predominantly pseudomorphic. Between 5 and 8 ML, the in-plane lattice constant is reduced by 4%, which corresponds to a reduction of the film strain by 70%. This is accompanied by an increasing interlayer spacing as predicted by elasticity theory. Kerr measurements show a perpendicular anisotropy between 5 and 12 ML and an in-plane magnetization below 5 and above 12 ML. The reorientation of magnetization is controlled by the film strain. To fully exploit the potential of tailoring magnetic films with perpendicular anisotropy, effective means to stabilize large film stress are highly desirable.

Acknowledgements

Fruitful collaboration with Y. Gauthier (Institut de Cristallographie, CNRS, Grenoble/France) and travel support within the PROCOPE program are gratefully acknowledged. This work was supported within the VDI project 'Magnetische Multischichten', Grant No. VDI 13N6607.

Appendix A. Calculations on the magnetic anisotropy

In the following we will derive an expression for the reorientation thickness of the magnetization of a thin epitaxial magnetic film. The relationship depends on the different contributions to magnetic anisotropy, such as magnetocrystalline, shape and magnetoelastic anisotropy. Both bulk and surface contributions have to be distinguished. The former grow linearly with the film thickness, while the surface contributions are independent of film thickness. We begin with the magnetocrystalline anisotropy of a cubic crystal, which writes

$$G^{\mathrm{V}}_{\mathrm{crystal}}(\Omega_{\mathrm{M}}) = K^{\mathrm{V}}_0 + K^{\mathrm{V}}_1(\alpha_1^2\alpha_2^2 + \alpha_2^2\alpha_3^2 + \alpha_3^2\alpha_1^2) + K^{\mathrm{V}}_2\alpha_1^2\alpha_2^2\alpha_3^2 + K^{\mathrm{V}}_3(\alpha_1^2\alpha_2^2 + \alpha_2^2\alpha_3^2 + \alpha_3^2\alpha_1^2)^2 + \cdots \tag{A.1}$$

for the volume contribution and

$$G^{\mathrm{S}}_{\mathrm{crystal}}(\Omega_{\mathrm{M}}) = K^{\mathrm{S}}_1 \sin^2\theta + (K^{\mathrm{S}}_2 + K'^{\mathrm{S}}_2 \cos(4\phi)) \sin^4\theta + \cdots \tag{A.2}$$

for the surface contribution. The coordinate system is oriented along the crystal axes. The magnetization vector $\boldsymbol{M}$ encloses the angle θ with the (0 0 1) surface normal and the angle ϕ with the [0 1 0]-direction. Thus, $\alpha_1 = \sin\theta\cos\phi$, $\alpha_2 = \sin\theta\sin\phi$ and $\alpha_3 = \cos\theta$. The anisotropy constants K in the sums have been determined by various experiments [21]. For the shape anisotropy energy of a thin plate of infinite extension we obtain

$$G^{\mathrm{V}}_{\mathrm{shape}} = K^{\mathrm{V}}_{\mathrm{shape}} \sin^2\theta, \tag{A.3}$$

which can be applied for ultrathin films. For the surface contribution of the shape anisotropy one finds

$$G^{\mathrm{S}}_{\mathrm{shape}} = K^{\mathrm{S}}_{\mathrm{shape}} \sin^2\theta. \tag{A.4}$$

Finally, we have the magnetoelastic contribution, where to our knowledge, only the volume terms are incorporated up to this time. The magnetoelastic energy for a cubic crystal writes

$$G_{\mathrm{magn.el}}(\Omega_{\mathrm{M}}, \varepsilon) = B_1(\varepsilon_{11}\alpha_1^2 + \varepsilon_{22}\alpha_2^2 + \varepsilon_{33}\alpha_3^2) + 2B_2(\varepsilon_{12}\alpha_1\alpha_2 + \varepsilon_{23}\alpha_2\alpha_3 + \varepsilon_{31}\alpha_3\alpha_1) + \cdots, \tag{A.5}$$

where B_1, B_2 are the magnetoelastic constants and the ε_{ii} are the strains in the films, i.e. the diagonal elements of the strain tensor ε. In this calculation we only consider systems, where the shear deformations ε_{ij} can be neglected. Consider now a tetragonal distorted unit cell with nearest-neighbour distance a in the tetragonal plane and lattice constant c in perpendicular direction. The nearest-neighbour distance of the undistorted cubic cell is denoted a_0. Then the strains in the plane are equal to the lattice mismatch f:

$$\varepsilon_{11} = \varepsilon_{22} = f = \frac{a - a_0}{a_0}. \tag{A.6}$$

The compression along the c-axis then yields

$$\varepsilon_{33} = \frac{c - a_0\sqrt{2}}{a_0\sqrt{2}} = \frac{c}{a_0\sqrt{2}} - 1. \tag{A.7}$$

Along the epitaxial line [6]

$$\frac{c}{c_0} = \left(\frac{a_0}{a}\right)^{\gamma}, \quad c_0 = a_0\sqrt{2}, \tag{A.8}$$

where c is a function of a. Replacing c, we obtain

$$\varepsilon_{33} = \left(\frac{a_0}{a}\right)^{\gamma} - 1, \quad \gamma = \frac{2c_{12}}{c_{11}}, \tag{A.9}$$

where c_{12}, c_{11} are the elastic constants. Now the magnetoelastic energy can be expressed in terms of the film lattice spacing

$$G_{\mathrm{magn.el}} = B_1\left\{\left(\frac{a}{a_0} - 1\right)\sin^2\theta + \left(\left(\frac{a_0}{a}\right)^{\lambda} - 1\right)\cos^2\theta\right\}. \tag{A.10}$$

For a film with a thickness of d monolayers we summarize the total magnetic anisotropy energy

$$G = d\left(G^{\mathrm{V}}_{\mathrm{crystal}} + G^{\mathrm{V}}_{\mathrm{shape}} + G^{\mathrm{V}}_{\mathrm{magn.el}}\right) + G^{\mathrm{S}}_{\mathrm{crystal}} + G^{\mathrm{S}}_{\mathrm{shape}}. \tag{A.11}$$

To simplify the expression, we neglect the volume contribution of the magnetocrystalline anisotropy. This can be justified for ultrathin metal films:

$$G = (K^{\mathrm{S}}_1 + K^{\mathrm{S}}_{\mathrm{shape}})\sin^2\theta + d\left(K^{\mathrm{V}}_{\mathrm{shape}}\sin^2\theta + B_1\left\{\left(\frac{a}{a_0} - 1\right)\sin^2\theta + \left(\left(\frac{a_0}{a}\right)^{\lambda} - 1\right)\cos^2\theta\right\}\right). \tag{A.12}$$

Replacing $\cos^2\theta$ by $(1 - \sin^2\theta)$, we obtain a linear function in $\sin^2\theta$, which can be differentiated with respect to θ to minimize energy. The first derivative of this function vanishes for values of $\theta = 0°$ and $\theta = 90°$. Within this approximation, we obtain an equation for the thickness d_{crit}, where a reorientation transition occurs, depending on the lattice constants of the film and substrate material:

$$d_{\mathrm{crit}} = \frac{-(K^{\mathrm{S}}_{\mathrm{shape}} + K^{\mathrm{S}}_{\mathrm{crystal}})}{K^{\mathrm{V}}_{\mathrm{shape}} + B_1(a/a_0 - (a/a_0)^{-2}(c_{12}/c_{11}))}. \tag{A.13}$$

To determine the reorientation thickness for a given epitaxial system a_0, a, one only needs to know the elastic constants and anisotropy constants [21] of the film material. An example is shown in Fig. 11, where the regions of in-plane and

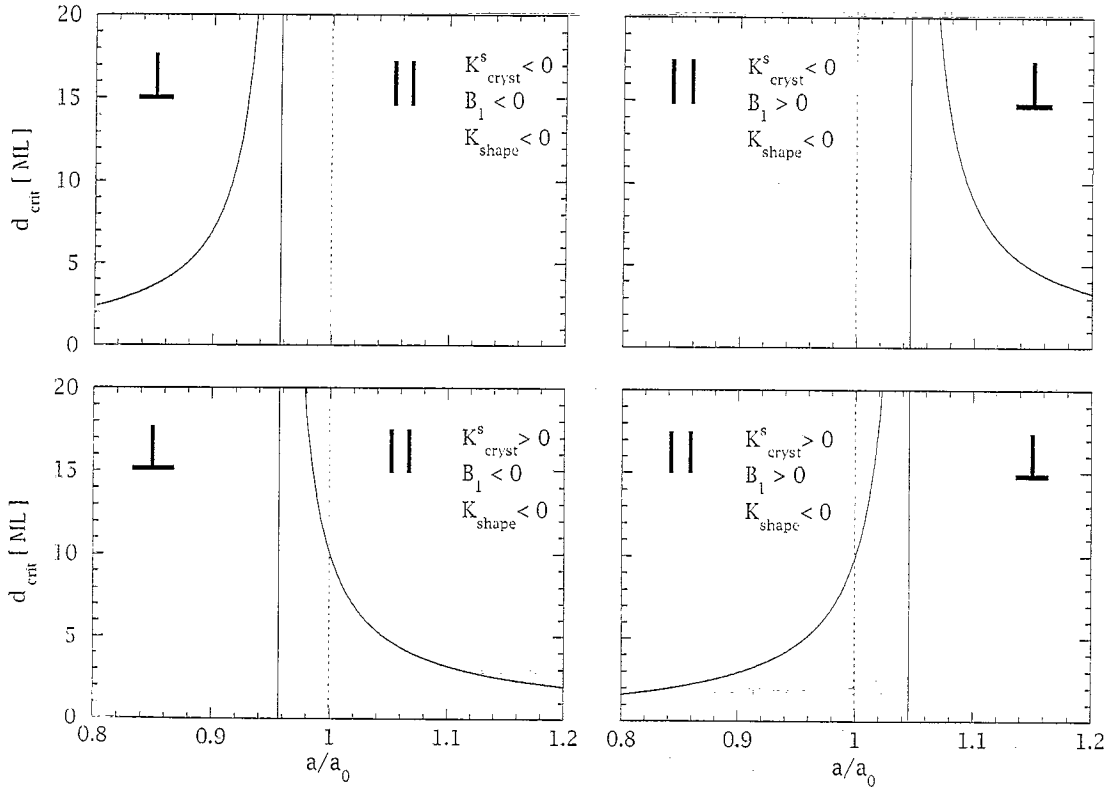

Fig. 11. Schematic diagram of the critical reorientation transition thickness d_{crit} for thin metal films, depending on the sign of the magnetic anisotropy constants, as estimated by Eq. (A.13). ⊥ denotes the phase area with perpendicular magnetization, and ‖ denotes the phase area with in-plane magnetization. The dotted line denotes the unstrained state in the film.

out-of-plane magnetization are displayed depending on the lattice mismatch and the sign of the anisotropy constants. Of course, it is also possible to take $G^V_{crystal}$ in account, but then the expression for the reorientation thickness becomes more complex.

References

[1] P. Bruno, J.-P. Renard, Appl. Phys. A 49 (1989) 499.
[2] W.L. O'Brien, B.P. Tonner, Phys. Rev. B 49 (21) (1994) 15370.
[3] B. Schulz, K. Baberschke, Phys. Rev. B 50 (18) (1994) 13467.
[4] G. Bochi, C.A. Ballentine, H.E. Inglefield, S.S. Bogomolov, C.V. Thompson, R.C. O'Handley, Mater. Res. Soc. Symp. Proc., vol. 313 (1993) 309.
[5] B. Feldmann, Ph.D. thesis, RWTH Aachen, 1996.
[6] P.M. Marcus, F. Jona, Surf. Rev. Lett. 1 (1) (1994) 15.
[7] J. Thomassen, B. Feldmann, M. Wuttig, Surf. Sci. 264 (1992) 406.
[8] M. Hansen, K. Anderko, Constitution of Binary Alloys, McGraw-Hill, New York, 1985.
[9] J.M. Van Hove, C.S. Lent, P.R. Pukite, P.I. Cohen, J. Vac. Sci. Technol. B 1 (1983) 741.
[10] J.H. Neave, B.A. Joyce, P.J. Dobson, N. Norton, Appl. Phys. A 47 (1985) 100.
[11] A. Berger, S. Knappmann, H.P. Oepen, J. Appl. Phys. 75 (1994) 5598.
[12] S. Knappmann, Diploma Thesis, Forschungszentrum Jülich, July 1994, unpublished.
[13] J. Thomassen, F. May, B. Feldmann, M. Wuttig, H. Ibach, Phys. Rev. Lett. 69 (1992) 3831.
[14] M. Henzler, Surf. Sci. 22 (1970) 12.
[15] M. Henzler, Appl. Phys. 9 (1976) 11.
[16] Y. Gauthier, A. Braun, B. Feldmann, M. Wuttig, to be published.

[17] G. Bochi, C.A. Ballentine, H.E. Inglefield, C.V. Thompson, R.C. O'Handley, H.J. Hug, B. Stiefel, A. Moser, H.-J. Güntherodt, Phys. Rev. B 52 (10) (1995) 7311.
[18] C. Chappert, P. Bruno, J. Appl. Phys. 64 (1988) 5736.
[19] J.W. Matthews, J. Vac. Sci. Technol. 12 (1) (1975) 126.
[20] W.D. Nix, Metall. Trans. A 20 (1989) 2217.
[21] For a collection of data see: J.A.C. Bland, B. Heinrich, Ultrathin Magnetic Structures, vols. I and II, Springer, Berlin, 1994.